

# A COMPREHENSIVE ANALYSIS OF *SWIFT* XRT DATA. I. APPARENT SPECTRAL EVOLUTION OF GAMMA-RAY BURST X-RAY TAILS

BIN-BIN ZHANG<sup>1,2</sup>, EN-WEI LIANG<sup>1,3</sup>, BING ZHANG<sup>1</sup>

*Draft version October 29, 2018*

## ABSTRACT

An early steep decay component following the prompt GRBs is commonly observed in *Swift* XRT light curves, which is regarded as the tail emission of the prompt gamma-rays. Prompted by the observed strong spectral evolution in the tails of GRBs 060218 and 060614, we present a systematic time-resolved spectral analysis for the *Swift* GRB tails detected between 2005 February and 2007 January. We select a sample of 44 tails that are bright enough to perform time-resolved spectral analyses. Among them 11 tails are smooth and without superimposing significant flares, and their spectra have no significant temporal evolution. We suggest that these tails are dominated by the curvature effect of the prompt gamma-rays due to delay of propagation of photons from large angles with respect to the line of sight. More interestingly, 33 tails show clear hard-to-soft spectral evolution, with 16 of them being smooth tails directly following the prompt GRBs, while the others being superimposed with large flares. We focus on the 16 clean, smooth tails and consider three toy models to interpret the spectral evolution. The curvature effect of a structured jet and a model invoking superposition of the curvature effect tail and a putative underlying soft emission component cannot explain all the data. The third model, which invokes an evolving exponential spectrum, seems to reproduce both the lightcurve and the spectral evolution of all the bursts, including GRBs 060218 and 060614. More detailed physical models are called for to understand the apparent evolution effect.

*Subject headings:* gamma-rays: bursts

## 1. INTRODUCTION

The extensive observations of gamma-ray bursts (GRBs) suggest that most of the broadband, power-law decaying afterglows are from external shocks as the fireball is decelerated by the ambient medium (Mészáros & Rees 1997a; Sari et al. 1998). The prompt gamma rays and the erratic X-ray flares after the GRB phase (Burrows et al. 2005), are instead of internal origin, likely from internal shocks (Rees & Mészáros 1994, see Zhang et al. 2006 for detailed discussion)<sup>4</sup>. The direct evidence for the distinct internal origin of prompt gamma-rays and X-ray flares is the steep decay tails following the prompt emission and the flares (Tagliaferri et al. 2005; Nousek et al. 2006; O’Brien et al. 2006), which could be generally interpreted as the so-called “curvature effect” due to the delay of propagation of photons from high latitudes with respect to the line of sight (Fenimore et al. 1996; Kumar & Panaitescu 2000; Qin et al. 2004; Dermer 2004; Zhang et al. 2006; Liang et al. 2006a). This clean picture

is somewhat “ruined” by some recent observations with *Swift*. A strong spectral evolution has been observed in the tails of two peculiar GRBs: 060218 (Campana et al. 2006; Ghisellini et al. 2006) and 060614 (Gehrels et al. 2006; Zhang et al. 2007b; Mangano et al. 2007), which is not directly expected from the curvature effect model. This suggests that there might be unrevealed emission components in the early afterglow phase. This motivates us to perform a systematic data analysis for both light curves and their spectral evolution of the GRB tails observed by *Swift*/XRT. Our data reduction and sample selection are delineated in §2. The light curves and spectral evolutions are presented in §3. In §4, we discuss three models, and identify an empirical model to interpret the data. Our conclusions are summarized in §5.

## 2. DATA REDUCTION AND SAMPLE SELECTION

The X-ray data are taken from the Swift data archive. We develop a script to automatically download and maintain all the Swift X-Ray Telescope (XRT) data. The Heasoft packages, including *Xspec*, *Xselect*, *Ximage*, and Swift data analysis tools, are used for the data reduction. We develop a set of IDL codes to automatically process the XRT data. The procedure is described as follows.

First, run the XRT tool *xrtpipeline* (Version 0.10.6) to reproduce the XRT clean event data, which have been screened with some correction effects (e.g. bad or hot pixels identifications, correct Housekeeping exposure times, etc.). The latest calibration data files (CALDB, released on Dec 06, 2006) are used.

Second, a time filter for the time-resolved spectral analysis is automatically performed. We initially divide the time series of XRT data into  $n$  (normally 30) equal segments in log-scale. Generally, these segments are not the real time intervals to perform the spectral analysis

<sup>1</sup> Department of Physics and Astronomy, University of Nevada, Las Vegas, NV 89154, USA; zbb@physics.unlv.edu; lew@physics.unlv.edu; bzhang@physics.unlv.edu

<sup>2</sup> National Astronomical Observatories/Yunnan Observatory, CAS, Kunming 650011, China

<sup>3</sup> Department of Physics, Guangxi University, Nanning 530004, China

<sup>4</sup> Most recently Ghisellini et al. (2007) suggested that most power-law decaying X-ray afterglows that show a shallow-to-normal decay transition are “late prompt emission” that is also of internal origin. The fact that most of the X-ray afterglows in the “normal” decay phase satisfy the well-known “closure relation” for the external shocks (Zhang et al. 2007a; see also the second paper in this series, Liang et al. 2007, Paper II), however, suggests that this is not demanded for most bursts. GRB 0070110, on the other hand, displays a flat X-ray emission episode followed by a rapid decay. This likely suggests an internal origin of the flat X-ray emission episode at least for some bursts (Troja et al. 2007).

because they may not have enough spectral bins to perform spectral fitting. A real time interval for our spectral analysis should satisfy two criteria, i.e., the spectral bins<sup>5</sup> in the time interval should be greater than 10, and the reduced  $\chi^2$  should be around unity. If one temporal segment does not satisfy our criteria, we combine the next time segment until the merged segment meets our criteria. With this procedure, we create a time filter array to perform time-resolved spectral analyses.

Third, make pile-up correction and exposure correction for each time interval. The pile-up correction is performed with the same methods as discussed in Romano et al. (2006) (for the Window Timing [WT] mode data) and Vaughan et al. (2006) (for the Photon Counting [PC] mode data). Both the source and the background regions are annuluses (for PC) or rectangular annuluses (for WT). For different time intervals, the inner radius of the (rectangular) annulus are dynamically determined by adjusting the inner radius of the annulus through fitting the source brightness profiles with the King's point source function (for PC) or determined by the photo flux using the method described in Romano et al. (2006) (for WT). If the pile-up effect is not significant, the source regions are in shape of a circle with radius  $R = 20$  pixels (for PC) or of a  $40 \times 20$  pixel<sup>2</sup> rectangle (for WT) centered at the bursts' positions. The background region has the same size as the source region, but is 20 pixels away from the source region. The exposure correction is made with an exposure map created by the XRT tools *artexpomap* for this given time interval.

Fourth, derive the corrected and background-subtracted spectrum and light curve for each time interval. The signal-to-noise ratio is normally 3, but we do not rigidly fix it to this value. Instead we adjust it if needed according to the source brightness at a given time interval.

Fifth, fit the spectrum in each time interval and convert the light curve in count rate to energy flux. The spectral fitting model is a simple power-law combined with the absorptions of both our Galaxy and the GRB host galaxy,  $wabs^{Gal} \times zwabs^{host} \times powerlaw$  (for bursts with known redshifts) or  $wabs^{Gal} \times wabs^{host} \times powerlaw$  (for bursts whose redshifts are unknown), except for GRB060218, for which a black body component is added to the fitting model,  $wabs^{Gal} \times wabs^{host} \times (powerlaw + bbbodyrad)$  (Campana et al. 2006)<sup>6</sup>. The  $nH^{Gal}$  value is taken from Dickey & Lockman (1990), while the  $nH^{host}$  is taken as a free parameter. We do not consider the variation of  $nH^{host}$  within a burst and fix this value to that derived from the time-integrated spectral fitting. With the spectrum in this time interval, we convert the photon flux to the energy flux.

We perform time-resolved spectral analyses with our code for all the Swift GRBs detected from Feb. 2005 to Jan. 2007, if their XRT data are available. We find

<sup>5</sup> We re-group the spectra using *grppha* in order to ensure a minimum of 20 counts per spectral bin

<sup>6</sup> We fix the parameters of the black body component to the same values as in Campana et al. (2006) (see also <http://www.brera.inaf.it/utenti/campana/060218/060218.html>). Please note that the XRT light curve of the first orbit is dominated by the black body component 2000 seconds since the GRB trigger. Therefore, the non-thermal emission in the first orbit is considered only for those before 2000 seconds since the GRB trigger.

that the X-rays of most GRBs are not bright enough to make time-resolved spectral analyses, i.e., only time-integrated spectra are derived. In this paper we focus on the spectral evolution of GRB tails. Therefore, our sample includes only those bursts that have bright GRB tails. All the tails studied have decay slopes  $\alpha < -2$ , and the peak energy fluxes in the tails are generally greater than  $10^{-9}$  erg cm<sup>-2</sup> s<sup>-1</sup>. Some GRB tails are superimposed with significant flares. Although it is difficult to remove the contamination of the flares, we nonetheless include these bursts as well in the sample. Our sample includes 44 bursts altogether. Their lightcurves and time-dependent spectral indices are displayed in Figs. 1-3.

### 3. RESULTS OF TIME-RESOLVED SPECTRAL ANALYSES

The light curves and spectral index evolutions of the GRB tails in our sample are shown in Figs. 1-3. For each burst, the upper panel shows the light curve and the lower panel shows the evolution of the spectral index  $\beta$  ( $\beta = \Gamma - 1$ , where  $\Gamma$  is the photon index in the simple power-law model  $N(E) \propto \nu^{-\Gamma}$ ). The horizontal error bars in the lower panel mark the time intervals. For the purpose of studying tails in detail, we zoom in the time intervals that enclose the tails. In order to compare the spectral behaviors of the shallow decay phase following the GRB tail, we also show the light curves and spectral indices of the shallow decay phase, if they were detected.

Shown in Fig.1 are those tails (Group A) whose light curves are smooth and free of significant flare contamination, and whose spectra show no significant evolution. The spectral indices of the shallow decay segment following these tails are roughly consistent with those of the tails. Figure 2 displays those tails (Group B) that have clear hard-to-soft spectral evolution<sup>7</sup>, but without significant flares (although some flickering has been seen in some of these tails). The spectral evolution of these tails should be dominated by the properties of the tails themselves, and this group of tails are the focus of our detailed modeling in §4. In contrast to the tails shown in Fig. 1, the spectra of the shallow decay components following these tails are dramatically harder than the spectra at the end of the tails. This indicates that the tails and the shallow decay components of these bursts have different physical origin.

The rest of the GRBs (about 1/3) in our sample show those tails (Group C) that are superimposed with significant X-ray flares. In most of these tails, strong spectral evolutions are also observed. These bursts are shown in Fig.3. Since the spectral behaviors may be complicated by the contributions from both the tails and the flares, modeling these tails is no longer straightforward, and we only present the data in Fig.3.

### 4. MODELING THE TAILS: AN EMPIRICAL SPECTRAL EVOLUTION MODEL

The physical origin of the GRB tails is still uncertain. In our sample, one-fourth of the tails do not show significant spectral evolution (Fig.1). The most straightforward interpretation for these tails is the curvature effect due to delay of propagation of photons from large angles with respect to the line of sight (Fenimore et al. 1996;

<sup>7</sup> We measure the spectral evolution of these bursts with  $\beta_{XRT} \propto \kappa \log t$ , and the  $\kappa$  values of these bursts are greater than 1.

Kumar & Painaitescu 2000; Wu et al. 2006). In this scenario, the decay is strictly a power law with a slope  $\alpha = -(2 + \beta)$  if the time zero point is set to the beginning of the rising segment of the lightcurve (Zhang et al. 2006, see Huang et al. 2002 for the discussion of time zero point in a different context). This model has been successfully tested with previous data (Liang et al. 2006a).

We show here that most of the tails in our sample have significant hard-to-soft spectral evolution (see Figs.2 and 3). The simplest curvature effect alone cannot explain this feature. We speculate three scenarios that may result in a spectral evolution feature and test them in turn with the data.

The first scenario is under the scheme of the curvature effect of a structure jet model. Different from the previous structured jet models (Mészáros, Rees & Wijers 1998; Zhang & Mészáro 2002; Rossi et al. 2002) that invoke an angular structure of both energy and Lorentz factor, one needs to assume that the spectral index  $\beta$  is also angle-dependent in order to explain the spectral evolution. Furthermore, in order to make the model work, one needs to invoke a more-or-less on axis viewing geometry. Nonetheless, this model makes a clear connection between the spectral evolution and the lightcurve, so that  $f^c(\nu, t) \propto [(t - t_p)/\Delta t + 1]^{-[2+\beta_c(t)]}\nu^{-\beta_c(t)}$ , where  $\beta_c(t)$  is the observed spectral evolution fitting with  $\beta_c(t) = a + \kappa \log t$ . We test this model with GRBs 060218 and 060614, the two typical GRBs with strong spectral evolution, and find that it fails to reproduce the observed light curves.

The second scenario is the superimposition of the curvature effect with a putative underlying power-law decay emission component. This scenario is motivated by the discovery of an afterglow-like soft component during  $10^4 - 10^5$  seconds in the nearby GRB 060218 (Campana et al. 2006). We process the XRT data of this component, and derive a decay slope  $-1.15 \pm 0.15$  and the power law photon spectral index  $4.32 \pm 0.18$ . This soft component cannot be interpreted within the external shock afterglow model (see also Willingale et al. 2007), and its origin is unknown. A speculation is that it might be related to the GRB central engine (e.g. Fan et al. 2006), whose nature is a great mystery. The most widely discussed GRB central engine is a black hole - torus system or a millisecond magnetar. In either model, there are in principle two emission components (e.g. Zhang & Mészáros 2004 and references therein). One is the “hot” fireball related to neutrino annihilation. This component tends to be erratic, leading to significant internal irregularity and strong internal shocks. This may be responsible for the erratic prompt gamma-ray emission we see. The second component may be related to extracting the spin energy of the central black hole (e.g. Blandford & Znajek 1977; Mészáros & Rees 1997b; Li 2000) or the spin energy of the central millisecond pulsar (through magnetic dipolar radiation, e.g. Usov 1992; Dai & Lu 1998; Zhang & Mészáros 2001). This gives rise to a “cold”, probably steady Poynting flux dominated flow. This component provides one possible reason to refresh the forward shock to sustain a shallow decay plateau in early X-ray afterglows (Zhang et al. 2006; Nousek et al. 2006), and it has been invoked to interpret the pecu-

liar X-ray plateau afterglow of GRB 070110 (Troja et al. 2007). These fact make us suspect that at least some of the observed spectrally evolving tails may be due to the superposition of a curvature effect tail and an underlying soft central engine afterglow<sup>8</sup>. In order to explain the observed hard-to-soft spectral evolution the central engine afterglow component should be much softer than the curvature effect component and it gradually dominates the observed tails. Analogous to forward shock afterglows, we describe the central engine afterglow component with

$$f^u(\nu, t) \propto t^{-\alpha_u} \nu^{-\beta_u}, \quad (1)$$

so that the total flux density can be modelled as

$$f(\nu, t) = f^c(\nu, t) + f^u(\nu, t), \quad (2)$$

where  $f^c(\nu, t)$  is the normal curvature effect component. The spectral index in the XRT band at a given time thus is derived through fitting the spectrum of  $\nu f_\nu(t)$  versus  $\nu$  with a power law, and the observed XRT light curve can be modeled by

$$F_{\text{XRT}}(t) = \int_{\text{XRT}} [f^c(\nu, t) + f^u(\nu, t)] d\nu. \quad (3)$$

We try to search for parameters to fit tails in our Group (B). Although the model can marginally fit some of the tails, we cannot find a parameter regime to reproduce both the lightcurves and observed spectral index evolutions for GRBs 060218 and 060614. We therefore disfavor this model, and suggest that the central engine afterglow emission, if any, is not significant in the GRB tails.

The third scenario is motivated by the fact that the broad-band data of GRB 060218 could be fitted by a cut-off power spectrum with the cutoff energy moving from high to low energy bands (Campana et al. 2006; Liang et al. 2006b). We suspect that our Group B tails could be of the similar origin. As a spectral break gradually passes the XRT band, one can detect a strong spectral evolution. We introduce an empirical model to fit the data. The time dependent flux density could be modeled as

$$F_\nu(E, t) = F_{\nu, m}(t) \left[ \frac{E}{E_c(t)} \right]^{-\beta} e^{-E/E_c(t)} \quad (4)$$

where

$$F_{\nu, m}(t) = F_{\nu, m, 0} \left( \frac{t - t_0}{t_0} \right)^{-\alpha_1} \quad (5)$$

and

$$E_c(t) = E_{c, 0} \left( \frac{t - t_0}{t_0} \right)^{-\alpha_2} \quad (6)$$

are the temporal evolutions of the peak spectral density and the cutoff energy of the exponential cutoff power law spectrum, respectively. In the model,  $t > t_0$  is required, and  $t_0$  is taken as a free parameter. Physically it should roughly correspond to the beginning of the internal shock emission phase, which is near the GRB trigger time. Our

<sup>8</sup> O’Brien et al. (2006) and Willingale et al. (2007) interpret the XRT lightcurves as the superpositions between a prompt component and the afterglow component. The putative central engine afterglow component discussed here is a third component that is usually undetectable but makes noticeable contribution to the tails.

fitted  $t_0$  values (Table 1) are typically 10-20 seconds, usually much earlier than the starting time of the steep decay tails, which are consistent with the theoretical expectation. The evolution of  $E_c$  has been measured for GRB 060218 (Campana et al. 2006; Ghisellini et al. 2006; Liang et al. 2006b; Toma et al. 2007). We first test this model with this burst. Our fitting results are shown in Fig. 4. We find that this model well explains the light curve and the spectral evolution of combined BAT-XRT data of GRB 060218. We therefore apply the model to both the light curves and spectral evolution curves of other Group B tails as well (Fig.2). We do not fit Group C tails (Fig.3) because of the flare contamination. Our fitting results<sup>9</sup> are displayed in Fig.2 and are tabulated in Table 1. The  $\chi^2$  and the degrees of the freedom of the fitting to the light curves are also marked in Fig.2. Although the flickering features in some light curves make the reduced  $\chi^2$  much larger than unity, the fittings are generally acceptable, indicating that this model is a good candidate to interpret the data. The distributions of the fitting parameters are shown in Fig.5. The typical  $E_{c,0}$  is about 90 keV at  $t_0 \sim 16$  seconds. The distribution of the peak spectral density decay index  $\alpha_1$  has more scatter than the  $E_c$  decay index  $\alpha_2$ . Interestingly it is found that  $\alpha_1$  is strongly correlated with  $\alpha$ , say,  $\alpha_1 = (0.82 \pm 0.10)\alpha - (1.00 \pm 0.38)$  (see Fig. 6; the quoted errors are at  $1\sigma$  confidence level.), with a Spearman correlation coefficient  $r = 0.90$  and a chance probability  $p < 10^{-4}$  ( $N = 16$ ). This is the simple manifestation of the effect that the faster a burst cool (with a steeper  $\alpha_1$ ), the more rapidly the tail drops (with a steeper  $\alpha$ ). The  $\alpha_2$  parameter is around 1.4 as small scatter. This indicates that the evolution behaviors of  $E_c$  are similar among bursts, and may suggest a common cooling process among different bursts.

Comparing the three scenarios discussed above, the third empirical model of the prompt emission region is the best candidate to interpret the spectral evolution of the Group B tails. The Group C tails may include additional (but weaker) heating processes during the decay phase (Fan & Wei 2005; Zhang et al. 2006), as have been suggested by the fluctuations and flares on the decaying tails. The steep decay component has been also interpreted as cooling of a hot cocoon around the jet (Pe'er et al. 2006). This model may be relevant to some tails of the long GRBs, but does not apply to the tails from the bursts of compact star merger origin (such as GRB 050724 and probably also GRB 060614, Zhang et al. 2007b). Another scenario to interpret the tails is a highly radiative blast wave that discharges the hadronic energy in the form of ultra-high energy cosmic ray neutrals and escaping cosmic-ray ions (Dermer 2007). It is unclear, however, whether the model can simultaneously interpret both the observed lightcurves and the spectral evolution curves of these tails. In addition, dust scattering may explain some features of the tails, including the spectral evolution, for some bursts (Shao & Dai 2007).

<sup>9</sup> In principle one should derive the parameters with the combined best fits to both the light curves and  $\beta$  evolutions. This approach is however impractical since the degrees of freedom of the two fits are significantly different. We therefore fit the light curves first, and then refine the model parameters to match the

Recently, Butler & Kocevski (2007) used the evolution of the hardness ratio as an indicator to discriminate the GRB tail emission and the forward shock emission. As shown in Fig.2, the spectra of the tails are significantly different from those of the shallow decay component. Spectral behaviors, including evolution of the hardness ratio, are indeed a good indicator to separate the two emission components. However, no significant difference was observed between the spectra of the tails and the following shallow decay component for the Group A bursts that show no significant spectral evolution (Fig.1).

With the observation by CGRO/BATSE, it was found that the prompt GRBs tend to show a spectral softening and a rapid decay (Giblin et al. 2002; Connaughton 2002). Ryde & Svensson (2002) found that about half of the GRB pulses for the BATSE data decay approximately as  $t^{-3}$ , and their  $E_p$ 's also decay as a power law. These results are consistent with the study of X-ray tails in this paper, suggesting a possible common origin of the spectral evolution of GRB emission.

## 5. CONCLUSIONS

We have systematically analyzed the time-dependent spectra of the bright GRB tails observed with *Swift*/XRT between Feb. 2005 and Jan. 2007. We select a sample of 44 bursts. Eleven tails (Group A) in our sample are smooth and without superimposing significant flares, and their spectra have no significant evolution features. We suggest that these tails are dominated by the curvature effect of the prompt gamma-rays. More interestingly, 33 tails in our sample show clear hard-to-soft spectral evolution, with 16 of them (Group B) being smooth tails directly following the prompt GRBs while the other 17 (Group C) being superimposed with significant flares. We focus on the Group B tails and consider three toy models to interpret the spectral evolution effect. We find that the curvature effect of a structured jet and the superposition model with the curvature effect and a putative underlying soft emission component cannot interpret all the data, in particular the strong evolution observed in GRB 060218 and GRB 060614. A third empirical model invoking an apparent evolution of a cutoff power law spectrum seems to be able to fit both the light curves and the spectral evolution curves of the Group B tails. More detailed physical models are called for to understand this apparent evolution effect.

We acknowledge the use of the public data from the Swift data archive. We thank an anonymous referee for helpful suggestions, and appreciate helpful discussions with Dai Z. G., Wang X. Y., Fan Y. Z., and Qin Y. P. This work is supported by NASA through grants NNG06GH62G, NNG06GB67G, NNX07AJ64G and NNX07AJ66G (for B.B.Z., E.W.L., B.Z.), and by the National Natural Science Foundation of China (for E.W.L.; grant 10463001).

spectral evolution behaviors. The  $\chi^2$  reported in Table 1 are calculated with the refined model parameters for the light curves. We cannot constrain the uncertainties and uniqueness of the model parameters with this method

## REFERENCES

- Blandford, R. D., & Znajek, R. L. 1977, MNRAS, 179, 433  
 Burrows, D. N., Romano, P., Falcone, A., Kobayashi, S., et al. 2005, Science, 309, 1833

TABLE 1: Fitting Results with the empirical model for Group B GRB Tails

GRB	$\alpha$	$E_{c,0}$ (keV)	$\beta$	$\alpha_1$	$\alpha_2$	$t_0$ (s)	$\chi^2$	$dof$
050421	2.8	70.2	-0.8	1.3	1.4	14.8	85.3	49
050724	2.2	83.8	0.3	0.4	1.6	25.8	221.6	113
050814	3.2	113.6	0.5	1.6	1.3	18.4	108.2	72
050915B	5.3	89.3	1.2	4.1	1.3	17.6	88.9	75
051227	2.5	62.0	0.4	1.1	1.5	36.9	32.6	19
060115	3.2	81.1	0.3	1.7	1.2	16.4	76.9	35
060211A	4.2	81.1	0.4	2.6	1.2	22.5	83.0	48
060218	2.2	113.9	0.2	1.1	1.0	75.5	273.0	211
060427	3.5	83.8	0.8	2.0	1.4	16.2	55.9	36
060428B	4.7	78.4	1.2	2.3	1.4	34.1	85.0	56
060614	3.3	127.6	0.0	1.8	1.4	17.6	871.0	618
060708	4.2	72.9	1.6	2.2	1.0	7.3	19.7	19
061028	4.6	75.6	0.0	3.4	1.0	25.0	49.9	30
061110A	4.8	83.8	0.7	2.4	1.2	6.8	52.5	48
061222A	4.7	64.7	1.2	2.3	1.3	22.5	57.3	45
070110	2.4	146.4	0.5	1.0	1.2	11.5	77.6	63

- Butler, N. R., & Kocevski, D. 2007, ApJ, submitted, (astro-ph/0702638)
- Campana, S., Mangano, V., Blustin, A. J., Brown, P., et al. 2006, Nature, 442, 1008
- Connaughton, V. 2002, ApJ, 567, 1028
- Dai, Z. G. & Lu, T. 1998, PhRvL, 81, 4301
- Dermer, C. D. 2004, ApJ, 614, 284
- Dermer, C. D. 2007, ApJ, in press (astro-ph/0606320)
- Dickey, J. M., & Lockman, F. J. 1990, ARA&A, 28, 215
- Fan, Y. Z. & Wei, D. M. 2005, MNRAS, 364, L42
- Fan, Y. Z., Piran, T., & Xu, D. 2006, JCAP, 9, 13
- Fenimore, E. E., Madras, C. D., & Nayakshin, S. 1996, ApJ, 473, 998
- Gehrels, N., Norris, J. P., Mangano, V., Barthelmy S. D., et al. 2006, Nature, 444, 1044
- Ghisellini, G., Ghirlanda, G., Mereghetti, S., Bosnjak, Z., et al. 2006, MNRAS, 372, 1699
- Ghisellini, G., Ghirlanda, G., Nava, L. & Firmani, C. 2007, ApJ, 658, L75
- Giblin, T. W., Connaughton, V., van Paradijs, J., Preece, R. D., Briggs, M. S., Kouveliotou, C., Wijers, R. A. M. J., & Fishman, G. J. 2002, ApJ, 570, 573
- Huang, Y. F., Dai, Z. G., & Lu, T. 2002, MNRAS, 332, 735
- Kumar, P. & Panaitescu, A. 2000, ApJ, 541, L51
- Li, L. X. 2000, ApJ, 531, L111
- Liang, E. W., Zhang, B., O'Brien, P. T., Willingale, R., et al. 2006a, ApJ, 646, 351
- Liang, E. W., Zhang, B.-B., Stamatikos, M., Zhang, B., et al. 2006b, ApJ, 653, L81
- Liang, E. W., Zhang, B.-B. & Zhang, B., 2007, ApJ, submitted (Paper II)
- Mangano, V., et al. 2007, A&A, in press, (astro-ph/0704.2235)
- Mészáros, P. & Rees, M. J. 1997a, ApJ, 476, 232
- Mészáros, P. & Rees, M. J. 1997b, ApJ, 482, L29
- Mészáros, P., Rees, M. J. & Wijers, R. A. M. J. 1998, ApJ, 499, 301
- Nousek, J. A., Kouveliotou, C., Grupe, D., Page, K. L., et al. 2006, ApJ, 642, 389
- O'Brien, P. T., Willingale, R., Osborne, J., Goad, M. R., et al. 2006, ApJ, 647, 1213
- Pe'er, A., Mészáros, P., & Rees, M. J. 2006, ApJ, 652, 482
- Qin, Y. P., Zhang, Z. B., Zhang, F. W., & Cui, X. H. 2004, ApJ, 617, 439
- Rees, M. J. & Mészáros, P. 1994, ApJ, 430, L93
- Romano, P., et al. 2006, A&A, 456, 917
- Rossi, E., Lazzati, D., & Rees, M. J. 2002, MNRAS, 332, 945
- Ryde, F., & Svensson, R. 2002, ApJ, 566, 210
- Sari, R., Piran, T., & Narayan, R. 1998, ApJ, 497, L17
- Tagliaferri, G., Goad, M., Chincarini, G., Moretti, A., et al. 2005, Nature, 436, 985
- Shao, L., & Dai, Z. G. 2007, ApJ, in press, (astro-ph/0703009)
- Toma, K., Ioka, K., Sakamoto, T., & Nakamura, T. 2007, ApJ, 659, 1420
- Troja, E., Cusumano, G., O'Brien, P., Zhang, B. et al, 2007, ApJ, inpress (astro-ph/0702220)
- Usov, V. V. 1992, Nature, 357, 472
- Vaughan, S., Goad, M. R., Beardmore, A. P., O'Brien, P. T. et al. 2006, ApJ, 638, 920
- Willingale, R., et al. 2007, ApJ, in press (astro-ph/0612031)
- Wu, X. F., Dai, Z. G., Wang, X. Y., Huang, Y. F., Feng, L. L., & Lu, T. 2006, 36th COSPAR Scientific Assembly, 36, 731
- Zhang, B. & Mészáros, P. 2001, ApJ, 552, L35
- Zhang, B. & Mészáros, P. 2002, ApJ, 571, 876
- Zhang, B. & Mészáros, P. 2004, IJMPA, 19, 2385
- Zhang, B., Fan, Y. Z., Dyks, J., Kobayashi, S., et al. 2006, ApJ, 642, 354
- Zhang, B., Liang, E., Page, K. L., Grupe, D. et al. 2007a, ApJ, 655, 989
- Zhang, B., Zhang, B. B., Liang, E. W., Gehrels, N., et al. 2007b, ApJ, 655, L25

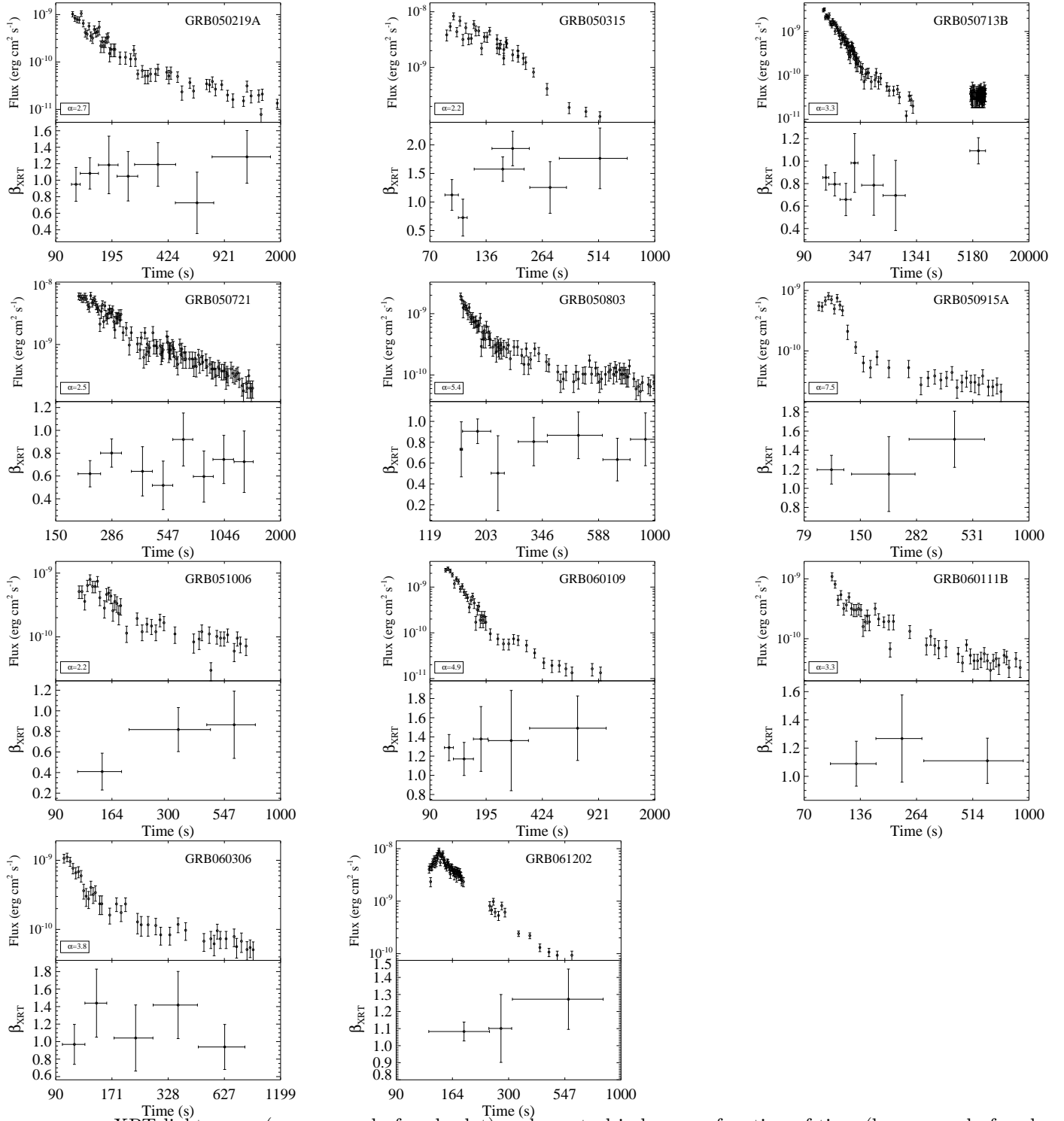


FIG. 1.— XRT light curve (upper panel of each plot) and spectral index as a function of time (lower panel of each plot) for those tails without significant spectral evolution (Group A). The horizontal error bars in the lower panels mark the time interval for the spectral analyses. Whenever available, the shallow decay segments following the tails and their spectral indices are also shown.

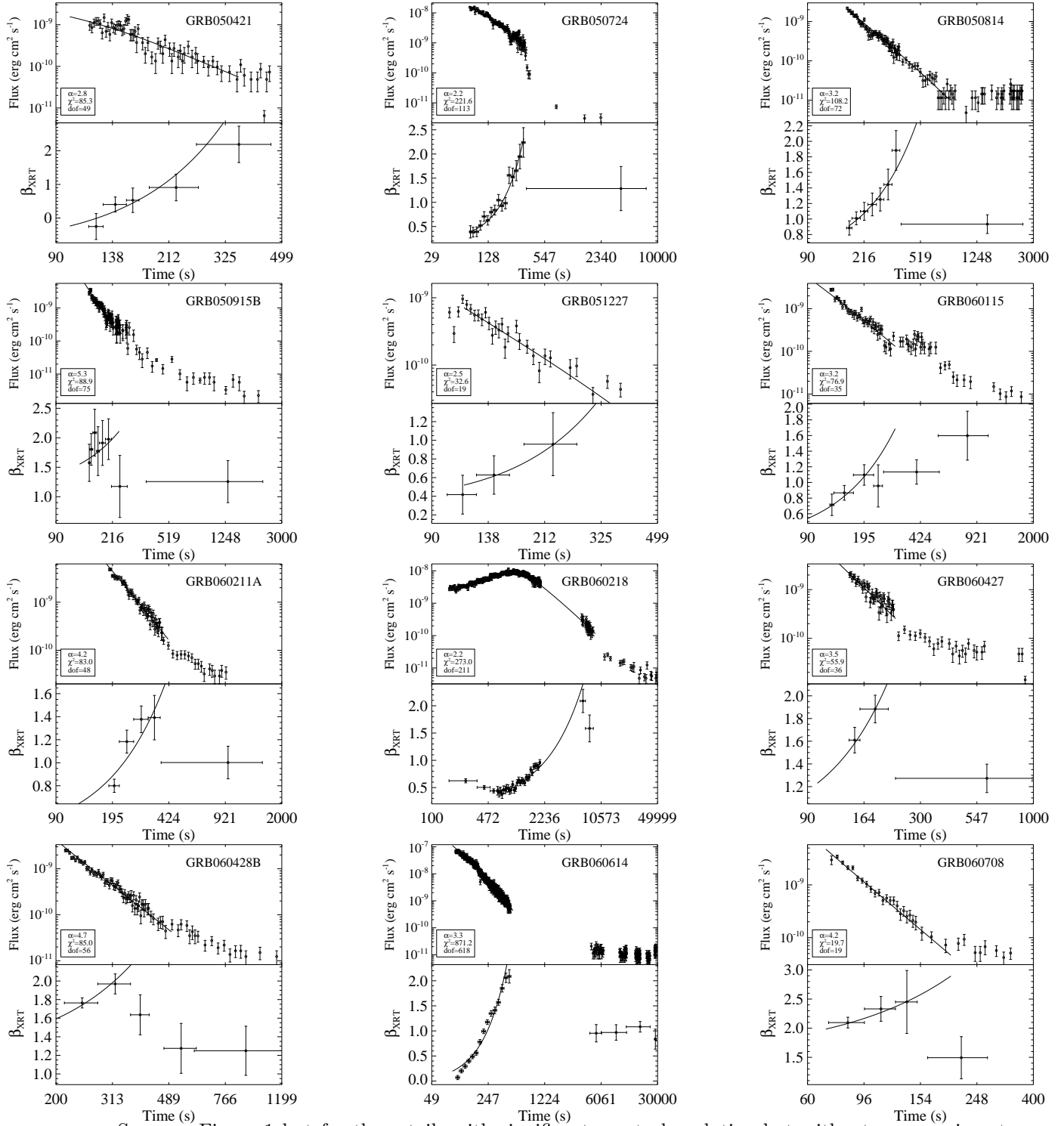


FIG. 2.— Same as Figure 1 but for those tails with significant spectral evolution but without superposing strong flares (Group B). The solid lines show the results of our proposed modeling.

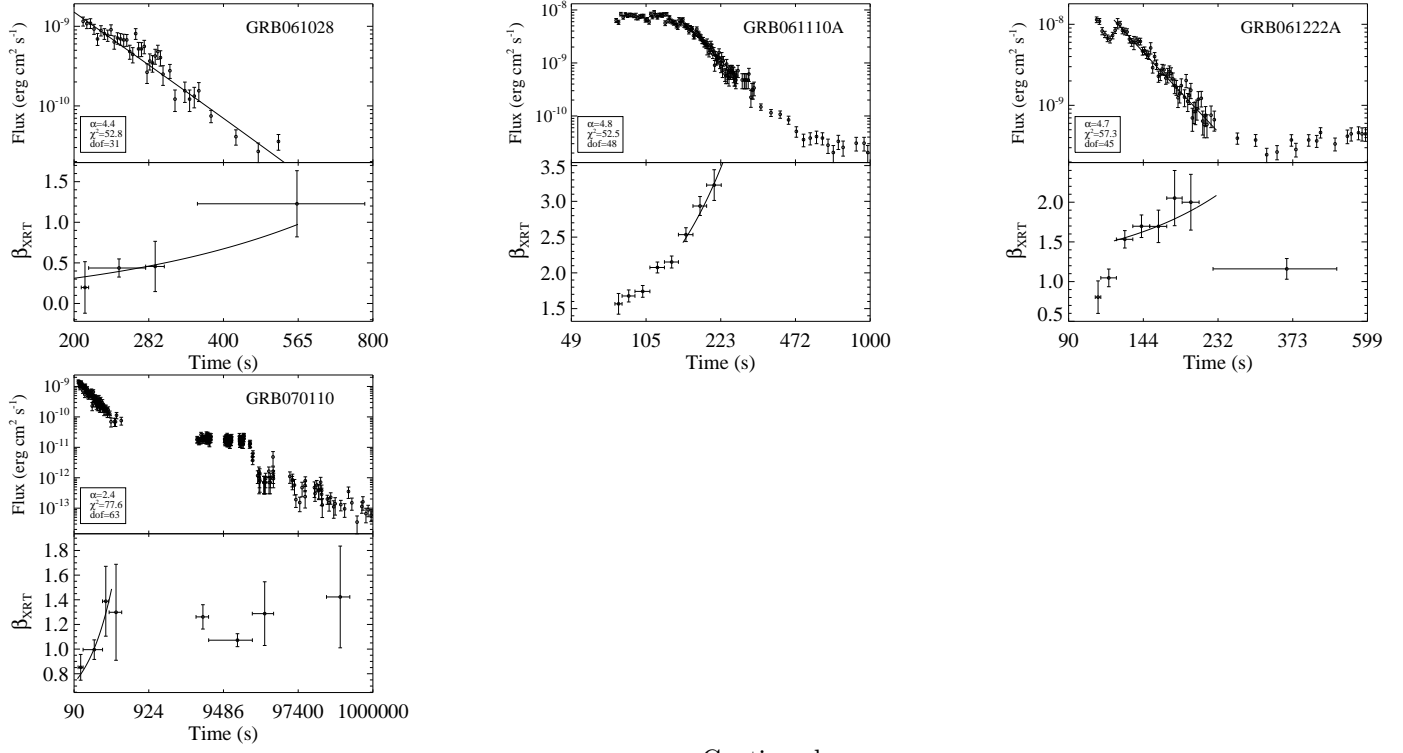


FIG. 2.—: Continued.



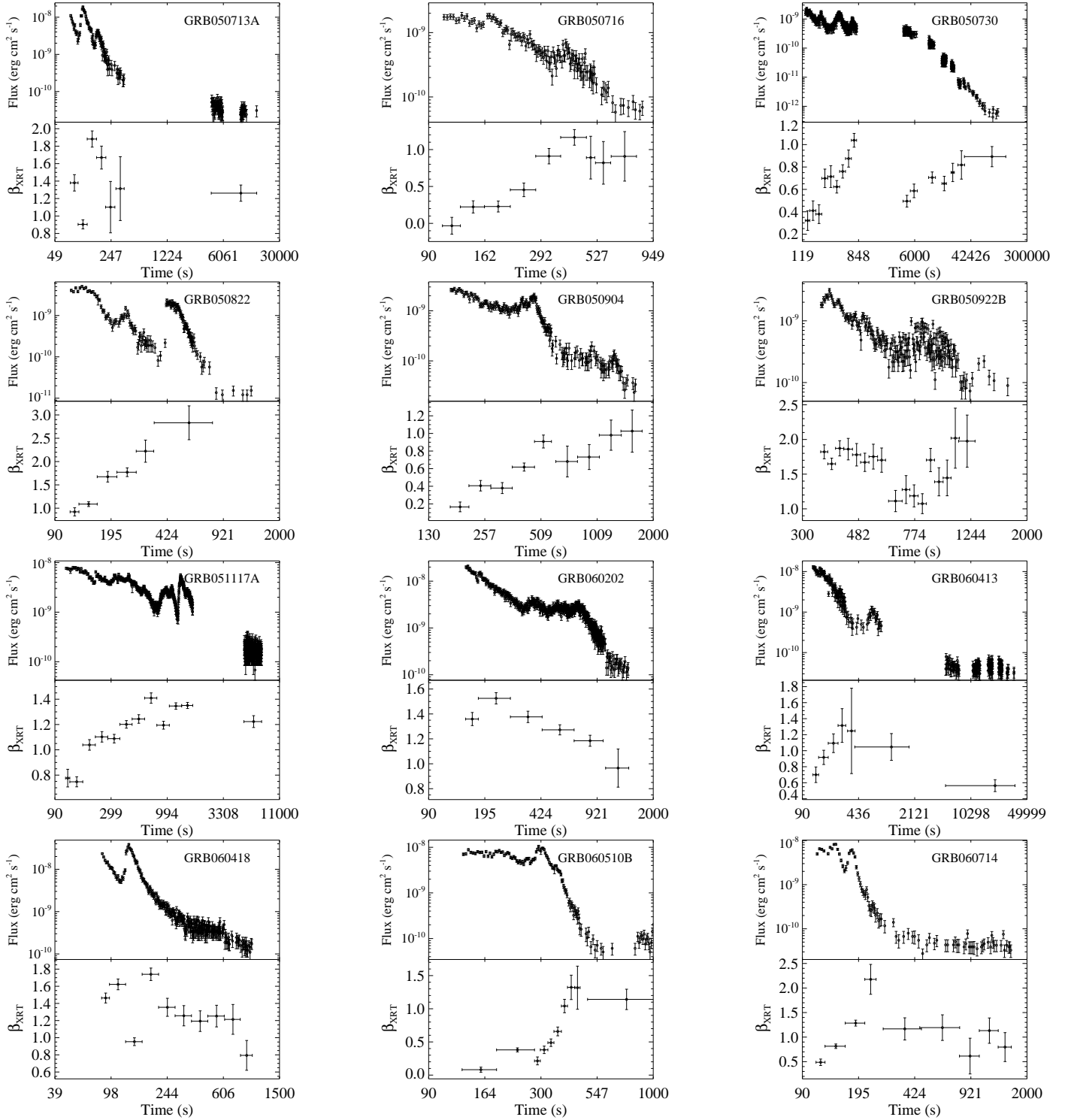


FIG. 3.— Same as Figure 1 but for those tails with significant flare contamination (Group C).

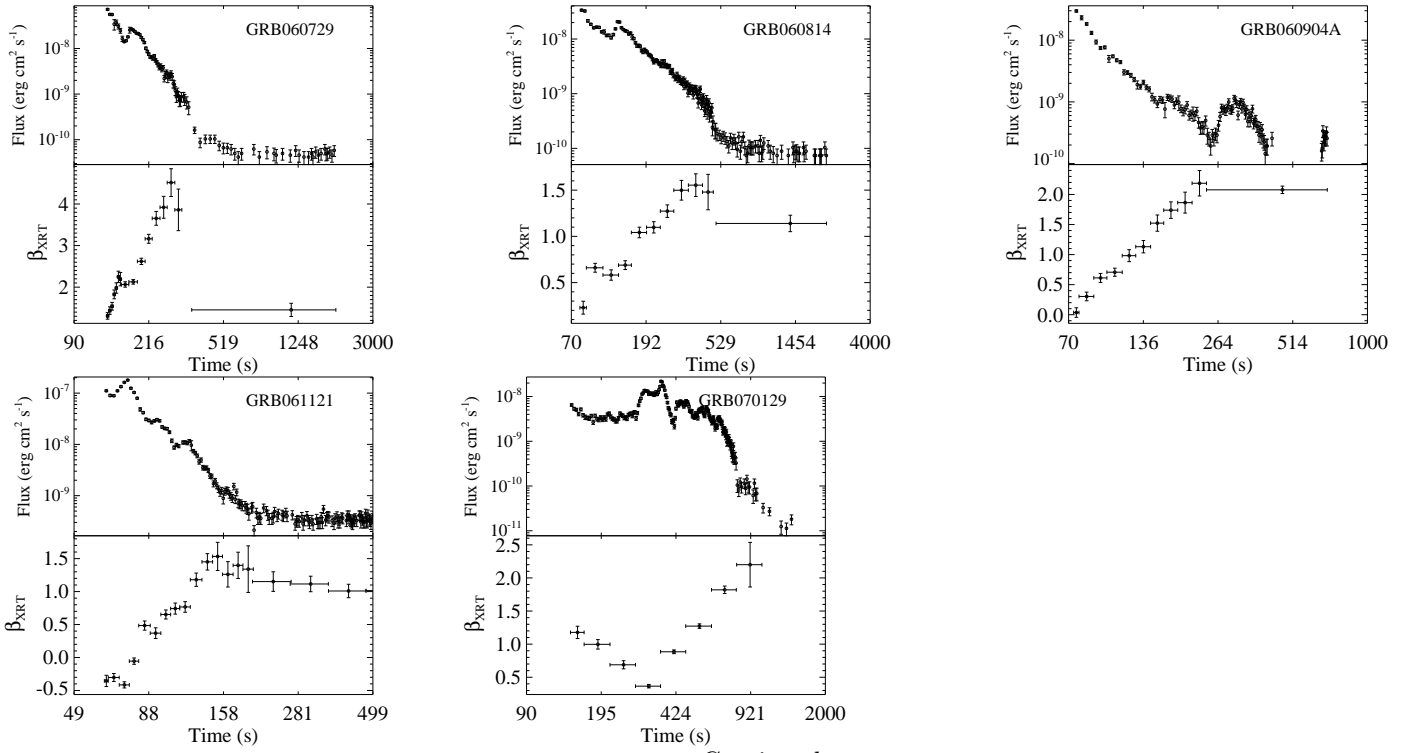


FIG. 3.—: Continued.

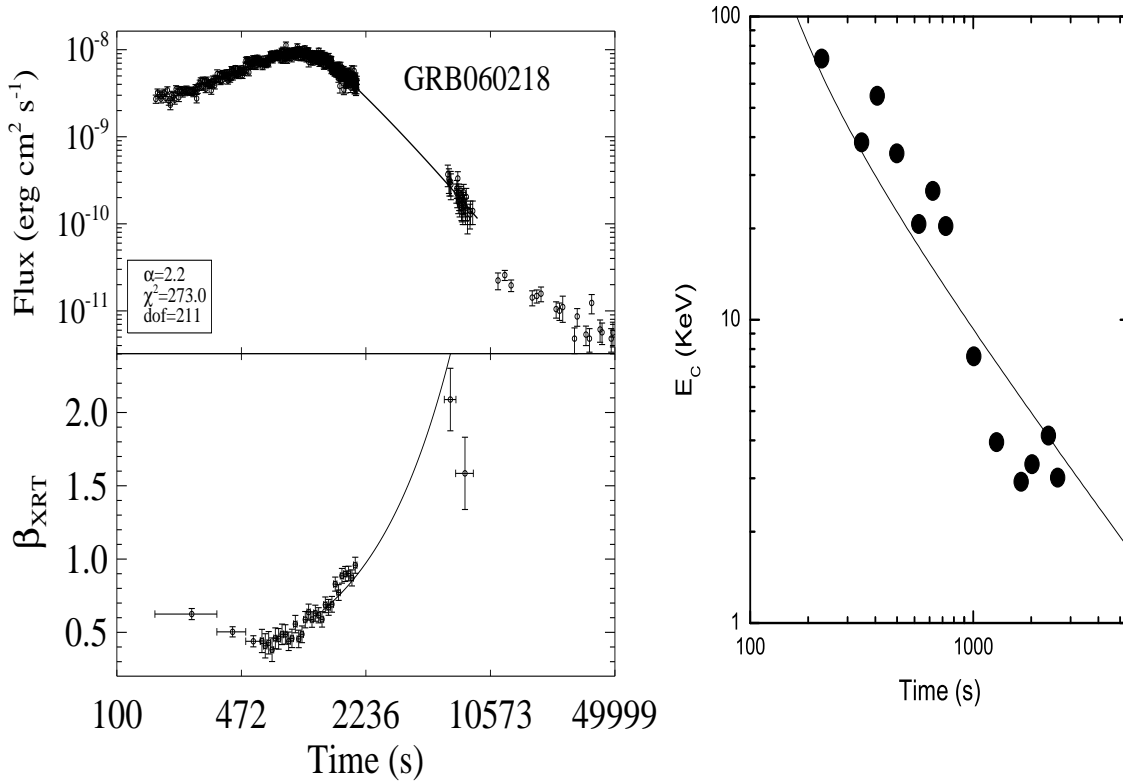


FIG. 4.—: Testing the third empirical model with the broad band data of GRB 060218. *Left*: Comparing the third empirical model prediction (solid lines) with the XRT lightcurve and the spectral evolution derived with the XRT data; *Right*: Comparing the third empirical model prediction (solid line) with the BAT/XRT joint-fit  $E_c$  evolution (circles, from Ghisellini et al. 2006, following Campana et al. 2006).

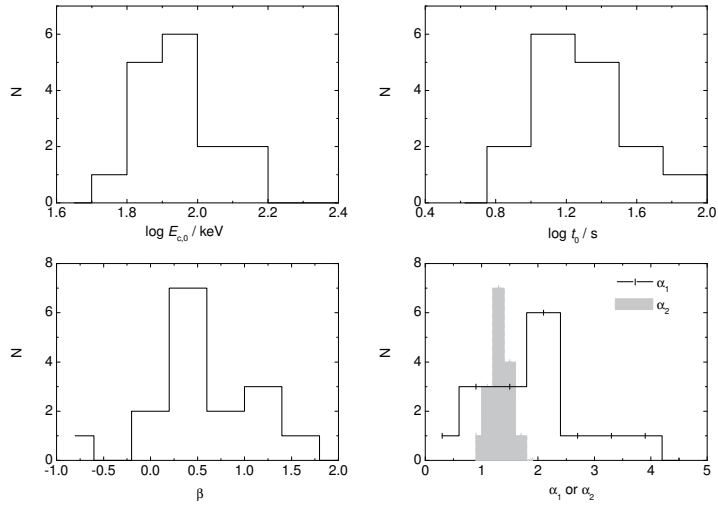


FIG. 5.—: Distributions of the model fitting parameters.

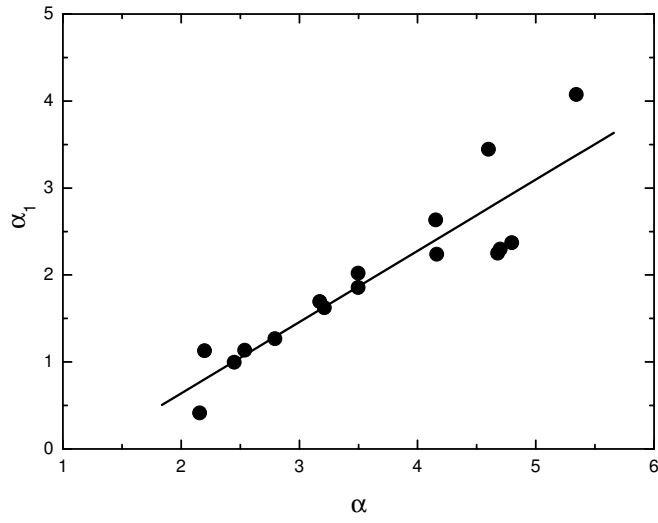


FIG. 6.— A correlation between the observed tail decay slope  $\alpha$  and the decay slope ( $\alpha_1$ ) of the “spectral amplitude” (defined in eq.[5]) for the 16 Group B bursts presented in Figure 2. The solid line is the regression line.